Please fill in the name of the event you are preparing this manuscript for.	SPE Reservoir Simulation Conference 2019				
Please fill in your 6-digit SPE manuscript number.	SPE-193817-MS				
Please fill in your manuscript title.	Von Neumann Stable, Implicit, High Order, Finite Volume WENO Schemes				

Please fill in your author name(s) and company affiliation.

Given Name	Surname	Company				
Todd	Arbogast	University of Texas at Austin, USA				
Chieh-Sen	Huang	National Sun Yat-sen University, Taiwan				
Xikai	Zhao	University of Texas at Austin, USA				

This template is provided to give authors a basic shell for preparing your manuscript for submittal to an SPE meeting or event. Styles have been included (Head1, Head2, Para, FigCaption, etc) to give you an idea of how your finalized paper will look before it is published by SPE. All manuscripts submitted to SPE will be extracted from this template and tagged into an XML format; SPE's standardized styles and fonts will be used when laying out the final manuscript. Links will be added to your manuscript for references, tables, and equations. Figures and tables should be placed directly after the first paragraph they are mentioned in. The technical content of your paper WILL NOT be changed. Please start your manuscript below.

### **Abstract**

Simulation of flow and transport in petroleum reservoirs involves solving coupled systems of advectiondiffusion-reaction equations with nonlinear flux functions, diffusion coefficients, and reactions/wells. It is important to develop numerical schemes that can approximate all three processes at once, and to high order, so that the physics can be well resolved. In this paper, we propose an approach based on high order, finite volume, implicit, Weighted Essentially NonOscillatory (iWENO) schemes. The resulting schemes are locally mass conservative and, being implicit, suited to systems of advection-diffusionreaction equations. Moreover, our approach gives unconditionally L-stable schemes for smooth solutions to the linear advection-diffusion-reaction equation in the sense of a von Neumann stability analysis. To illustrate our approach, we develop a third order iWENO scheme for the saturation equation of two-phase flow in porous media in two space dimensions. The keys to high order accuracy are to use WENO reconstruction in space (which handles shocks and steep fronts) combined with a two-stage Radau-IIA Runge-Kutta time integrator. The saturation is approximated by its averages over the mesh elements at the current time level and at two future time levels; therefore, the scheme uses two unknowns per grid block per variable, independent of the spatial dimension. This makes the scheme fairly computationally efficient, both because reconstructions make use of local information that can fit in cache memory, and because the global system has about as small a number of degrees of freedom as possible. The scheme is relatively simple to implement, high order accurate, maintains local mass conservation, applies to general computational meshes, and appears to be robust. Preliminary computational tests show the potential of the scheme to handle advection-diffusion-reaction processes on meshes of quadrilateral gridblocks, and to do so to high order accuracy using relatively long time steps. The new scheme can be viewed as a generalization of standard cell-centered finite volume (or finite difference) methods. It achieves high order in both space and time, and it incorporates WENO slope limiting.

### Introduction

Standard finite volume methods used widely in reservoir simulators are accurate to relatively low order. They may achieve second order results on uniform computational grids, but they will generally revert to first order on general grids. In some applications, one would like more resolution of the underlying physics, and so higher order numerical methods may be preferred. In particular, one might want improved capturing of shocks or steep fronts.

Many approaches have been proposed to increase the order of approximation. These include the mixed finite element methods (e.g., Durlovsky & Chien 1993; Hoteit & Firoozabadi 2008; Zidane & Firoozabadi 2018), mimetic methods (e.g., Alpak 2007; Guevara-Jordan & Jhonnanthan 2007; Alpak 2010; Nilsen et al. 2012), and discontinuous Galerkin methods (Riviere et al. 2011; Wang et al. 2015; Lee & Wheeler 2017; Zidane & Firoozabadi 2018). These methods require many degrees of freedom to achieve higher order approximation, and the degrees of freedom are *internal* to the grid block.

Other approaches use one degree of freedom per grid block, such as the multipoint flux methods (e.g., Chen et al. 2007; Parramore et al. 2013; Souza et al. 2018; Wheeler et al. 2012), which have been developed for subsurface simulation. They achieve higher order approximation through *reconstruction* of fluxes using neighboring degrees of freedom. An alternative but similar approach was developed for fluid dynamics applications involving hyperbolic conservation laws, namely, the Weighted Essentially NonOscillatory (WENO) schemes (Harten et al. 1987; Liu et al. 1994; Jiang & Shu 1996). These have seen limited application to reservoir simulation (see, e.g., Mallison et al. 2003). The advantage of schemes that use a single degree of freedom per grid block is that they maximize the grid resolution. This is important in resolving heterogeneities in the rock properties, especially, the permeability and porosity. Rather than using multiple degrees of freedom within each grid block, which would reduce the resolution of the heterogeneities, multipoint flux and WENO methods use a finer grid but achieve high order through reconstruction of the solution.

Properly posed finite volume schemes will be locally mass conservative. Unfortunately, it is not possible to define high order methods that preserve the maximum principle, i.e., that produce saturations between 0 and 1 (or, more precisely, greater than or equal to the residual values). It is not even possible to define low order methods that preserve the maximum principle on general unstructured computational meshes. Some slope limiting procedure is required to limit the oscillation. WENO methods have a slope limiting procedure based on reduction to lower order methods, which generally satisfy the maximum principle better (at the expense of adding numerical diffusion into the solution). They are not strictly nonoscillatory, but they are *essentially* nonoscillatory.

In this paper, we explore the potential of WENO schemes for petroleum reservoir simulation. As a prototype, we develop an implicit WENO (iWENO) scheme for the saturation equation of two-phase flow in porous media in two space dimensions with a single rock type. The pressure equation will be solved using a mixed finite element method. The saturation equation is a degenerate parabolic equation, meaning that the capillary diffusion term vanishes at the residual saturations. Even though advection dominates diffusion, so the equation is nearly hyperbolic, the diffusive term requires the use of implicit time stepping. We will use the two-stage, third order, implicit Radau-IIA Runge-Kutta method. This method is L-stable, meaning it is well suited to stiff problems involving diffusion. It leads to unconditionally stable schemes in the sense of a von Neumann stability analysis (Peaceman 1977).

We exploit some recent developments in WENO technology. Traditional WENO reconstructs the cell averages of the saturation into low order polynomials of some fixed degree on several stencils. It combines these by automatically weighting away from stencils that cross shocks or steep fronts in the saturation. Special weights need to be used so that the approximation is higher order when there are no shocks. To define these weights requires rectangular computational grids, and sometimes even uniform grids. The WENO reconstructions of Adaptive Order (WENO-AO) (Levy et al. 1999; Arbogast et al. 2018) do not require special weights. Instead of combining only low order polynomials, a polynomial of

higher degree is included directly. One consequence of this approach is that it frees one from rectangular computational meshes. We will describe procedures for meshes of quadrilaterals.

We will also exploit some recent developments in mixed method technology for the pressure equation. The lowest order mixed finite element method is equivalent to a cell-centered finite difference method on rectangular grids (Russell & Wheeler 1983). However, on quadrilateral grids, the method loses accuracy. This was rectified recently by the introduction of new finite element spaces on quadrilaterals (Arbogast & Correa 2016; Arbogast & Tao 2019).

Extension of our approach to three space dimensions, three phase systems, and to higher than third order should be straightforward. Extension to the pressure equation and multiple rock types may require more research.

## **Mathematical Formulation for Two-Phase Flow**

The equations describing two-phase flow in a petroleum reservoir are well known (see, e.g., Peaceman 1977; Lake 1989; Chen et al. 2006). For simplicity of exposition, we will take constant densities, vanishing residual saturations, constant porosity, and a single rock type. In that case, we can formulate the two-phase flow problem as a simple elliptic pressure equation and a parabolic, but nearly hyperbolic, saturation equation. The way this is done is by defining the *global pressure* (Chavent and Jaffré 1986; Arbogast 1992), which is a pressure intermediate between the two phase pressures. It can be defined by

$$p = p_n + \int_{S_w}^1 \lambda_w(S) \, p_c'(S) \, / \, \lambda(S) \, dS, \qquad (1)$$

where  $\lambda_w(S_w)$  is the relative mobility. Then,  $\lambda(S_w)\nabla p = \lambda_n(S_w)\nabla p_n + \lambda_w(S_w)\nabla p_w$ , and the pressure equation is posed for the total velocity  $\boldsymbol{u}$  as

$$\boldsymbol{u} = -K \lambda(S_w)[\nabla p - \rho(S_w)\boldsymbol{g}], \quad \dots \qquad (2)$$

$$\nabla \cdot \boldsymbol{u} = q(S_w), \quad \dots \qquad (3)$$

where  $q(S_w) = q_w(S_w) + q_n(S_w)$  is the total well source term and  $\lambda(S_w)\rho(S_w) = \lambda_w(S_w)\rho_w + \lambda_n(S_w)\rho_n$ .

The saturation equation is the mass conservation equation of one of the phases. If we choose the wetting fluid, this equation is

$$\phi \frac{\partial}{\partial t} S_w + \nabla \cdot [f_w(S_w) \boldsymbol{u} - \gamma(S_w) \boldsymbol{g} - D(S_w) \nabla S_w] = q_w(S_w), \qquad (4)$$

where 
$$f_w(S_w) = \lambda_w(S_w) / \lambda(S_w)$$
,  $\gamma(S_w) = K (\rho_n - \rho_w) \lambda_w(S_w) \lambda_n(S_w) / \lambda(S_w)$ , and  $D(S_w) = -K p_c'(S_w) \lambda_w(S_w) \lambda_n(S_w) / \lambda(S_w)$ .

# A Mixed Finite Element Method for the Pressure Equation

The global pressure equation (2)-(3) allows us to solve for the global pressure p and total velocity u independently of the saturation equation (4), assuming  $S_w$  is given. One can solve (2)-(3) in a number of ways; we chose to use a mixed finite element method.

We introduce a computational mesh of quadrilaterals over the reservoir domain. For this mesh, we can define the recently introduced AC mixed finite element spaces (Arbogast & Correa 2016; see also Arbogast & Tao 2018; Arbogast & Tao 2019). For a scalar test function w and a vector test function v in the AC space, we take the dot product of (2) with v and the product of (3) with w and integrate over the domain. After applying the Divergence Theorem, we obtain, for time level n,

$$\iint (K \lambda(S_w^n))^{-1} \boldsymbol{u}^n \cdot \boldsymbol{v} \, dx \, dy = \iint [p^n \nabla \cdot \boldsymbol{v} + \rho(S_w^n) \, \boldsymbol{g} \cdot \boldsymbol{v}] \, dx \, dy, \quad \dots \qquad (5)$$

Given  $S_w^n$ , we solve these equations for  $u^n$  and  $p^n$  in the same AC space. Since the purpose of this paper is to describe the iWENO framework for solving the saturation equation, we omit the details of implementation and refer the reader to the aforementioned references.

For consistency, we should use the AC space of index 2 (AC<sub>2</sub>), so that we achieve third order. However, the pressure is smoother than the saturation, so perhaps one might choose to take a lower index space. We do so in the numerical results that we present later in the paper.

# An Implicit WENO Method for the Saturation Equation

To discretize the saturation equation (4), we will use the same computational mesh. This is not strictly necessary, as any mesh of polytopes would suffice. However, by using the same mesh, we avoid the problem of projecting the solution of (2)-(3) onto the saturation mesh, and projecting  $S_w$  onto the pressure mesh. Let E be a generic mesh cell or *element*, and let |E| denote its area. Let E have E facets, denoted  $\partial E_l$ , E and E being its length. Finally, let E denote the maximum of the diameters of the mesh elements, and assume that the mesh is quasi-uniform, so E and E are E are E being its length.

The average of  $S_w$  over E at time t is denoted

$$\bar{S}_E(t) = \frac{1}{|E|} \iint_E S_w(x, y, t) dx dy.$$
 (7)

We integrate (4) over the element E and apply the Divergence Theorem to obtain

$$\phi_{dt}^{\underline{d}} \bar{S}_{E} + \frac{1}{|E|} \sum_{l=1}^{L} \int_{\partial E_{l}} [f_{w}(S_{w}) \boldsymbol{u} - \gamma(S_{w}) \boldsymbol{g} - D(S_{w}) \nabla S_{w}] \cdot v_{l} \, ds \, (x, y) = \frac{1}{|E|} \iint_{E} q_{w}(S_{w}) \, dx \, dy, \quad \dots \quad (8)$$

where  $v_l$  is the outward unit normal to the *l*-th facet of the boundary of *E*.

We approximate each boundary integral using a 2-point Gauss quadrature rule with points  $(x_{l,k},y_{l,k})$  and weights  $|\partial E_l| \omega_{l,k}$ , k=1,2. To simplify the notation, we define  $F(S_w) = f_w(S_w) \mathbf{u} - \gamma(S_w) \mathbf{g}$ , which is the hyperbolic flux, and then on facet  $\partial E_l$ , the first two terms in the boundary integral of (8) become

$$\frac{1}{|E|} \int_{\partial E_{l}} [f_{w}(S_{w}) \boldsymbol{u} - \gamma(S_{w}) \boldsymbol{g}] \cdot \nu_{l} ds (x, y) = \frac{1}{|E|} \int_{\partial E_{l}} \boldsymbol{F}(S_{w}) \cdot \nu_{l} ds (x, y)$$

$$= \frac{|\partial E_{l}|}{|E|} \sum_{k=1}^{2} \omega_{l,k} \widehat{F}_{l}(S_{w}^{-}, S_{w}^{+}) (x_{l,k}, y_{l,k}) + O(h^{3}), \qquad (9)$$

where  $\hat{F}_l$  is the numerical flux function for  $F \cdot v_l$ . We use the Lax-Friedrichs flux, which is given by

$$\widehat{F}_{l}(S_{w}^{-}, S_{w}^{+}) = \frac{1}{2} [(F(S_{w}^{-}) + F(S_{w}^{+})) \cdot \nu_{l} - \delta(S_{w}^{+} - S_{w}^{-})], \quad \dots$$
 (10)

where  $\delta$  is an upper bound for the absolute value of the eigenvalues of the Jacobian of F in the direction of  $v_l$ , and  $S_w^-$  and  $S_w^+$  are reconstructed values of  $S_w$  inside the element and in the neighboring element at the quadrature point, respectively (we will explain how to get these values in the next section). The third term in the boundary integral of (8), i.e., the diffusive capillary flux, can be approximated on  $\partial E_l$  by

$$\frac{1}{|E|} \int_{\partial E_l} D(S_w) \nabla S_w \cdot v_l \ ds \ (x,y) = \frac{|\partial E_l|}{|E|} \sum_{k=1}^2 \omega_{l,k} \ \widehat{D}_l(S_w^-, S_w^+) (x_{l,k}, y_{l,k}) \ S_{v,l}(x_{l,k}, y_{l,k}) + O(h^3), \ \dots \dots (11)$$

wherein a reconstructed value  $S_{v,l}$  of  $\nabla S_{w} \cdot v_l$  at the quadrature points is used (we will explain how to get these values in the next section). We again use a Lax-Friedrichs flux  $\widehat{D}_l$  for D, but now the parameter  $\delta$  is the maximum of  $|D'(S)\nabla S \cdot v_l|$ . The integration of the source term  $q_w(S_w)$  over E is evaluated to third order by tensor product 2-point Gauss quadrature (applied through mapping points from a reference square). That is, for the four quadrature points  $(x_k, y_k)$  and weights  $|E|\omega_k$ , k=1,2,3,4,

$$\frac{1}{|E|} \iint_{E} q_{w}(S_{w}) dx dy = \sum_{k=1}^{4} \omega_{k} q_{w}(S_{w}(x_{k}, y_{k})) + O(h^{3}), \qquad (12)$$

where  $S_w$  at the quadrature points must be reconstructed as described in the next section.

Combining (8)-(12), we must solve in time the equation

$$\phi_{dt}^{\underline{d}} \bar{S}_{E} = -\frac{1}{|E|} \sum_{l=1}^{L} \sum_{k=1}^{2} |\partial E_{l}| \omega_{l,k} [\widehat{F}_{l}(S_{w}^{-}, S_{w}^{+})(x_{l,k}, y_{l,k}) + \widehat{D}_{l}(S_{w}^{-}, S_{w}^{+})(x_{l,k}, y_{l,k}) S_{\nu,l}(x_{l,k}, y_{l,k})] 
+ \sum_{k=1}^{4} \omega_{k} q_{\nu}(S_{\nu}(x_{k}, y_{k})). \qquad (13)$$

One could solve this equation to lower order using backward Euler or Crank-Nicolson time discretization. However, for consistency, we choose to solve in time to third order.

One would like to use a Strong Stability Preserving (SSP) Runge-Kutta method for the time evolution (Gottlieb et al. 2001; Gottlieb 2005; Ketcheson et al. 2009). However, there are no unconditionally stable SSP methods of higher order, and the time step restriction is comparable to the CFL condition of explicit methods. This makes them unsuitable for two-phase flow.

An A-stable Runge-Kutta method is stable for the test equation y' = ay, where a < 0. That is,  $y^{n+1} = Q(\Delta t)y^n$ , and  $|Q(\Delta t)| \le 1$ . However, when the differential equation is stiff, it is possible that  $\Delta t$  is relatively large for the stiff components. An L-stable Runge-Kutta method is A-stable and satisfies  $\lim_{\Delta t \to \infty} |Q(\Delta t)| = 0$ ; that is, the stiff components contribute little (as they should) when the time step is large. Since (13) has stiff components, especially from the capillary diffusion term, we use an L-stable Runge-Kutta method. We remark that backward Euler is L-stable, but Crank-Nicolson is only A-stable.

Perhaps the simplest third order L-stable Runge-Kutta method is the Radau-IIA method (Hairer & Wanner 1996; Hairer et al. 2006). The Butcher Tableau for this two stage method is given in Table 1. We illustrate the method for the differential equation du/dt = f(u). Given the solution  $u^n$  at time  $t^n$ , one solves implicitly for the solution

Table 1: Butcher Tableau for Radau-IIA.

 $u^{n+1/3}$  and  $u^{n+1}$  at times  $t^{n+1/3} = t^n + \Delta t/3$  and  $t^{n+1} = t^n + \Delta t$  by solving the two equations

$$u^{n+1/3} = u^n + \frac{\Delta t}{12} \left[ 5f(t^{n+1/3}, u^{n+1/3}) - f(t^{n+1}, u^{n+1}) \right], \qquad (14)$$

$$u^{n+1} = u^n + \frac{\Delta t}{4} \left[ 3f(t^{n+1/3}, u^{n+1/3}) + f(t^{n+1}, u^{n+1}) \right]. \qquad (15)$$

The application of Radau-IIA time stepping to (13) results in finding approximations  $\bar{S}_E^{n+1/3}$  at time  $t^{n+1/3}$  and  $\bar{S}_E^{n+1}$  at time  $t^{n+1}$  satisfying the two equations

$$\phi \bar{S}_{E}^{n+1/3} = \phi \bar{S}_{E}^{n} - \frac{\Delta t}{12|E|} \sum_{l=1}^{L} \sum_{k=1}^{2} |\partial E_{l}| \omega_{l,k} \{$$

$$5[\hat{F}_{l}(S_{w}^{n+1/3,-}, S_{w}^{n+1/3,+}) (x_{l,k,y_{l,k}}) + \hat{D}_{l}(S_{w}^{n+1/3,-}, S_{w}^{n+1/3,+}) S_{v,l}^{n+1/3} (x_{l,k,y_{l,k}})]$$

$$-[\hat{F}_{l}(S_{w}^{n+1,-}, S_{w}^{n+1,+}) (x_{l,k,y_{l,k}}) + \hat{D}_{l}(S_{w}^{n+1,-}, S_{w}^{n+1,+}) S_{v,l}^{n+1} (x_{l,k,y_{l,k}})] \}$$

$$+ \frac{\Delta t}{12} \sum_{k=1}^{4} \omega_{k} [5q_{w}(S_{w}^{n+1/3}(x_{k,y_{k}})) - q_{w}(S_{w}^{n+1}(x_{k,y_{k}}))], \qquad (16)$$

$$\phi \bar{S}_{E}^{n+1} = \phi \bar{S}_{E}^{n} - \frac{\Delta t}{4|E|} \sum_{l=1}^{L} \sum_{k=1}^{2} |\partial E_{l}| \omega_{l,k} \{$$

$$3[\hat{F}_{l}(S_{w}^{n+1/3,-}, S_{w}^{n+1/3,+}) (x_{l,k,y_{l,k}}) + \hat{D}_{l}(S_{w}^{n+1/3,-}, S_{w}^{n+1/3,+}) S_{v,l}^{n+1/3} (x_{l,k,y_{l,k}})]$$

$$+ [\hat{F}_{l}(S_{w}^{n+1,-}, S_{w}^{n+1,+}) (x_{l,k,y_{l,k}}) + \hat{D}_{l}(S_{w}^{n+1,-}, S_{w}^{n+1,+}) S_{v,l}^{n+1} (x_{l,k,y_{l,k}})] \}$$

$$+ \frac{\Delta t}{4} \sum_{k=1}^{4} \omega_{k} [3q_{w}(S_{w}^{n+1/3}(x_{k,y_{k}})) + q_{w}(S_{w}^{n+1}(x_{k,y_{k}}))]. \qquad (17)$$

These equations must be solved implicitly, using, e.g., Newton's method. The saturation  $S_w$  must be evaluated at specific quadrature points (at the two time levels). WENO3 reconstruction is used to relate these values to the primary unknowns  $\bar{S}_E^{n+1/3}$  and  $\bar{S}_E^{n+1}$  on E and its neighboring grid elements.

## **WENO-AO Reconstructions**

We now describe the WENO-AO reconstructions needed to complete the iWENO3 scheme (16)-(17).

#### WENO-AO(3,2) Reconstruction in One Dimension.

We describe our basic WENO-AO(3,2) reconstruction in one space dimension (Levy et al. 1999; Arbogast et al. 2018) before discussing two dimensions. Partition space into a grid of points ...  $< x_{-1} < x_0$ 

 $< x_1 < \dots$ , and define the element interval  $I_i = [x_i, x_{i+1}]$  and its length  $h_i = x_{i+1} - x_i$ . The average of S(x) on  $I_i$  is denoted  $\bar{S}_i$ . We reconstruct S(x) for some  $x \in I_i$  from the element averages.

First, we define three polynomials approximating S(x). Let  $P_L(x)$  be a linear polynomial defined to the left of  $I_i$  by requiring its averages to match those of S on the stencil  $\{I_{i-1}, I_i\}$ , i.e.,  $\bar{P}_{L,i-1} = \bar{S}_{i-1}$  and  $\bar{P}_{L,i} = \bar{S}_i$ . Let  $P_R(x)$  be a linear polynomial defined to the right of  $I_i$  by requiring  $\bar{P}_{R,i} = \bar{S}_i$  and  $\bar{P}_{R,i+1} = \bar{S}_{i+1}$  for the stencil  $\{I_i, I_{i+1}\}$ . Finally, let  $P_0(x)$  be a quadratic polynomial defined on the full stencil  $\{I_{i-1}, I_i, I_{i+1}\}$  by requiring  $\bar{P}_{0,i-1} = \bar{S}_{i-1}$ ,  $\bar{P}_{0,i} = \bar{S}_i$ , and  $\bar{P}_{0,i+1} = \bar{S}_{i+1}$ . Provided that S is smooth on the big stencil,  $P_0$  is a third order approximation to S(x), while the other two polynomials are second order.

We select *arbitrary* positive weights  $\alpha_L$ ,  $\alpha_R$ , and  $\alpha_0 = 1 - (\alpha_L + \alpha_R)$  (say, 0.25, 0.25, and 0.5) to combine the three polynomials. We modify the weights nonlinearly according to the smoothness of the polynomials on the element  $I_i$ , which are measured using the standard smoothness indicator (Jiang & Shu 1996). For polynomial P(x), it is given by

$$\sigma_P = \sum_{k=1}^2 \int_{I_i} h_i^{2k-1} \left[ \frac{d^k}{dx^k} P(x) \right]^2 dx. \qquad (18)$$

Define

$$\hat{\alpha}_k = \frac{\alpha_k}{(\varepsilon + \sigma_{P_k})^2}, \quad \tilde{\alpha}_k = \frac{\hat{\alpha}_k}{\hat{\alpha}_L + \hat{\alpha}_0 + \hat{\alpha}_R}, \quad k = L, 0, R, \dots (19)$$

where  $\varepsilon = 1\text{E-}6$  is usually taken (but see Arandiga et al. 2011 and Arbogast et al. 2018 for a discussion of this parameter). We combine the three polynomials to define our reconstruction R(x) as

$$S(x) \approx R(x) = \frac{\tilde{\alpha}_0}{\alpha_0} [P_0(x) - \alpha_L P_L(x) - \alpha_R P_R(x)] + \tilde{\alpha}_L P_L(x) + \tilde{\alpha}_R P_R(x). \qquad (20)$$

If S is smooth on the stencil of three elements, the smoothness indicators are very small and so  $S \approx P_0$  is a third order approximation. If S is not smooth to the left,  $\sigma_L$  and  $\sigma_0$  become O(1), and so  $S \approx P_R$  is second order, and if S is not smooth to the right,  $S \approx P_L$  is second order. Notice that WENO-AO used arbitrary weights, reconstructed any point in the interval  $I_i$ , and did not require a uniform grid.

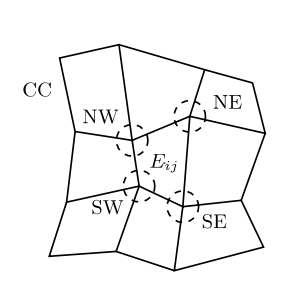
#### **WENO-AO(3,2)** Reconstruction in Two Dimensions.

WENO reconstructions on unstructured meshes in two dimensions are available (see, e.g., Hu & Shu 1999; Titarev et al. 2010). However, we choose to develop a reconstruction tailored to logically rectangular meshes of quadrilaterals. That is, the mesh is a distortion of a rectangular mesh, and so the index space may be taken to be rectangular. Given an element  $E_{ij}$ , let  $(x_{ij}, y_{ij})$  be its centroid. For numerical stability, one should let  $h = \sqrt{|E_{ij}|}$  and work in the local variables  $(x - x_{ij})/h$  and  $(y - y_{ij})/h$ , but for simplicity of exposition we will continue with the variables x and y.

As shown in Figure 1, consider four small 2×2 stencils

SE = {
$$E_{i,j}$$
,  $E_{i+1,j}$ ,  $E_{i,j-1}$ ,  $E_{i+1,j-1}$ }, SW = { $E_{i,j}$ ,  $E_{i-1,j}$ ,  $E_{i,j-1}$ ,  $E_{i-1,j-1}$ }, NE = { $E_{i,j}$ ,  $E_{i+1,j}$ ,  $E_{i,j+1}$ ,  $E_{i+1,i+1}$ }, NW = { $E_{i,j}$ ,  $E_{i-1,j}$ ,  $E_{i,j+1}$ ,  $E_{i-1,j+1}$ },

and the big 3×3 stencil CC of their union. We construct a bilinear polynomial  $P_k$ , k = SE, SW, NE, NW, by matching the averages of the polynomial over each element in its stencil to the corresponding saturation averages, i.e., so that  $\bar{P}_{p,q}$  agrees with  $\bar{S}_{E_{ij},p,q}$  for the appropriate p,q in the stencil (at whatever time level we need the reconstruction). We also construct the biquadratic polynomial  $P_{CC}$  similarly for the stencil CC.



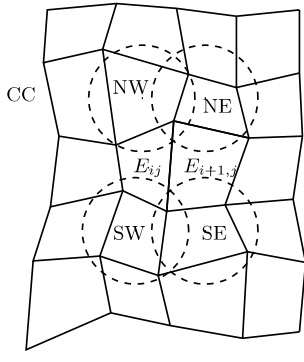


Fig. 1. Left: Stencils used for WENO-AO(3,2) reconstructions on  $E_{ij}$ . Right: Stencils used for WENO-AO(4,3) reconstructions needed on  $E_{ij} \cap E_{i+1,j}$  for the capillary diffusion term.

For a time dependent problem with a fixed computational mesh, a good way to implement the procedure above is to first define the base polynomials (Aràndiga et al. 2011), for which the saturation data is all zeros, except for a single one. Given a small or big stencil k, let  $\hat{P}_{k,p,q}(x,y)$  be defined such that

$$\frac{1}{|E_{p'q'}|} \int_{E_{p'q'}} \hat{P}_{k,p,q}(x,y) \, dx \, dy = \begin{cases} 1, & p = p', q = q', \\ 0, & \text{otherwise,} \end{cases}$$
 (21)

which can be precomputed once the mesh is given. The stencil polynomial is then

$$P_k(x,y) = \sum_{p,q} \bar{S}_{E_{pq}} \hat{P}_{k,p,q}(x,y).$$
 (22)

This technique greatly simplifies the definition of polynomials and smoothness indicators, as well as the computation of the Jacobian needed in Newton's method.

For any point in the central element, i.e., for  $(x,y) \in E_{ij}$ , the WENO-AO(3,2) reconstruction is

$$R(x,y) = \frac{\tilde{\alpha}_{CC}}{\alpha_{CC}} \left[ P_{CC}(x,y) - \sum_{k} \alpha_{k} P_{k}(x,y) \right] + \sum_{k} \tilde{\alpha}_{k} P_{k}(x,y), \dots$$
 (23)

where the sum is over the values of k representing the small (2×2) stencils and the *linear* weights  $\alpha_k$  are arbitrary positive numbers summing up to 1 (we take 1/8 for the four small stencils and 1/2 for the big one). The *nonlinear* weights  $\tilde{\alpha}_k$  and  $\tilde{\alpha}_{CC}$  are defined analogously to (19), once the smoothness indicator is defined. We define it (Hu & Shu 1999) for the polynomial P on degree N by

$$\sigma_P = \sum_{k=1}^{N} \sum_{l=0}^{k} |E_{ij}|^{k-1} \int_{E_{ij}} \left[ \frac{d^l}{dx^l} \frac{d^{k-l}}{dy^{k-l}} P(x, y) \right]^2 dx dy, \qquad (24)$$

and simplify it using pairs of the base polynomials by computing

$$\sigma_{P,pq}^{p'q'} = \sum_{k=1}^{N} \sum_{l=0}^{k} |E_{ij}|^{k-l} \int_{E_{ij}} \frac{d^{l}}{dx^{l}} \frac{d^{k-l}}{dy^{k-l}} \hat{P}_{k,p,q}(x,y) \frac{d^{l}}{dx^{l}} \frac{d^{k-l}}{dy^{k-l}} \hat{P}_{k,p',q'}(x,y) dx dy \qquad (25)$$
and setting

$$\sigma_P = \sum_{pq} \sum_{p'q'} \bar{S}_{E_{p'q'}} \bar{S}_{E_{p'q'}} \sigma_{P,pq}^{p'q'}. \qquad (26)$$

We use (23) for all reconstructions of  $S_w$  at a point of the grid element  $E_{ij}$ . On the boundary, we have  $S_w^-$ , and  $S_w^+$  comes from the reconstruction on the neighboring element.

## WENO-AO(4,3) Reconstruction in Two Dimensions for the capillary diffusion.

The reconstruction of the normal derivatives  $S_{\nu,l}(x,y)$  on facet  $\partial E_l = E_{ij} \cap E_{i+1,j}$  (or  $E_{ij} \cap E_{i,j+1}$ ) is formed by differentiation of the reconstruction polynomial, which must then be one power higher order accurate. For stability, it must also be defined in a symmetric way. We use a WENO-AO(4,3) procedure analogous to the WENO-AO(3,2) procedure described above. As depicted in Fig. 1 for  $\partial E_l = E_{ij} \cap E_{i+1,j}$ , the big stencil, CC, has  $4 \times 5$  grid elements and its associated tensor product polynomial  $P_{\text{CC}}$  is

third order in x and fourth order in y. The four small stencils are  $3\times3$  and lie in the corners of the big stencil, and their associated tensor product polynomials are biquadratic. The reconstruction is

for a point  $(x,y) \in \partial E_l$ , where the sum is over the values of k representing the small (3×3) stencils.

# **Properties of the iWENO3 Scheme**

The iWENO3 scheme is a generalization of standard cell-centered finite volume (or finite difference) methods. It is locally mass conservative by design. It is formally third order accurate in both space and time, although one might choose to implement it with less temporal accuracy when most of the error is spatial. The scheme reverts to second order accuracy in space near shocks and steep fronts. It is not nonoscillatory, but essentially so due to the WENO slope limiting mechanism.

The scheme can be shown to be stable in terms of a von Neumann stability analysis. One must apply the analysis to the linearized version of the saturation equation (4), and assume that the saturation is smooth. The latter assumption means that the reconstructions will be given by the big stencil polynomials. Moreover, one must assume a uniform computational grid. The analysis shows that each Fourier mode is L-stable (see Arbogast et al. 2018 technical report).

The saturation is approximated by its averages over the mesh elements, and so the scheme maximizes the grid resolution. It requires solving for unknown average saturations at two future time levels per grid block. For systems of M unknowns, we would need only two unknowns per grid block per variable, independent of the spatial dimension. The scheme is not particularly difficult to implement and it is fairly computationally efficient, both because reconstructions use local information that can fit in cache memory, and because the global system has about as small a number of degrees of freedom as possible.

# **Numerical Results for Simple Test Problems**

In this section, we give results for our iWENO3 scheme in one and two space dimensions for three simple test problems. We show the accuracy and robustness of the scheme. Newton's method is used to solve the iWENO3 scheme for the differential equation of the test problem, and we use the sparse direct matrix solver in the Eigen library (Gaël, Benoît, et al. 2010).

For conciseness of expressing the differential equations, we will use the convention that a subscript consisting of a variable (t, x, or y) will denote partial differentiation.

### **Example 1: Buckley-Leverett Equation.**

The first example uses the scalar equation  $u_t + (f(u))_x = 0$  with the nonconvex Buckley-Leverett flux function

$$f(u) = \frac{u^2}{u^2 + (1-u)^2}.$$
 (28)

The initial condition

$$u_0(x) = \begin{cases} 1 - 20x, & \text{for } 0 \le x \le 0.05, \\ 0.5, & \text{for } 0.25 \le x \le 0.4, \\ 0, & \text{otherwise,} \end{cases}$$
 (29)

leads to an interaction of shocks and rarefactions, i.e., two pulses merge over time. We use m = 80 grid elements. The results are shown in Fig. 2. The scheme handles the merging of the two pulses quite well and reproduces the solution to adequate accuracy.

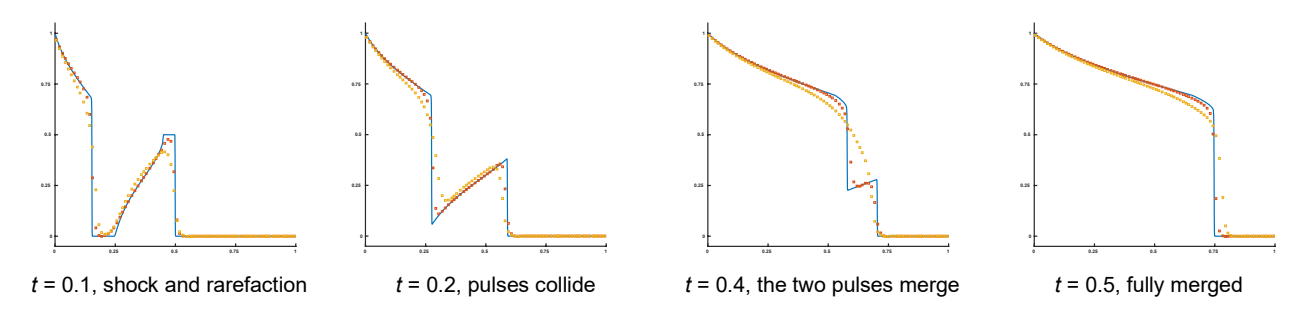


Fig. 2: Buckley-Leverett equation. The blue solid line is the reference solution. The red squares are iWENO3 results on nonuniform meshes using m = 80 and  $\Delta t = h$ . The orange squares are backward Euler results.

We also compare results using a backward Euler time stepping procedure combined with a second order (i.e., linear approximation) iWENO2 scheme. The low order method shows much greater numerical diffusion. It also reduces to a single pulse much earlier than the true and iWENO3 solutions.

### **Example 2: Burgers' Equation with Diffusion.**

We now consider Burgers' equation with linear diffusion,

$$u_t + (u^2/2)_x - Du_{xx} = 0.$$
 (30)

Exact solutions can be found using the Hopf-Cole transformation, and we take the exact solution

$$u(x,t) = \frac{-2D\pi \cos(\pi x)\exp(-D\pi^2 t)}{2+\sin(\pi x)\exp(-D\pi^2 t)}.$$
 (31)

We show results for D=0.1 and D=0.01 in Table 2 on nonuniform grids using  $\Delta t=10.5h$ . We see the expected third order convergence rates, in both the  $L^1$  and  $L^{\infty}$  norms. It should be noted that the CFL number for this problem is 1, so 10.5 is a considerable improvement over explicit methods.

	D = 0.1				D = 0.01			
m	L <sup>1</sup> error	order	L <sup>∞</sup> error	order	L1 error	order	L <sup>∞</sup> error	order
80	3.74E-05		3.13E-05		9.42E-06		1.69E-05	
160	5.01E-06	2.90	4.23E-06	2.89	1.18E-06	3.00	2.06E-06	3.03
320	6.36E-07	2.98	5.40E-07	2.97	1.47E-07	3.01	2.49E-07	3.05
640	8.10E-08	2.97	6.90E-08	2.97	1.84E-08	3.00	3.14E-08	2.99
1280	1.02E-08	2.99	8.66E-09	2.99	2.30E-09	3.00	3.91E-09	3.00

Table 2: Burgers' equation with exact solution (31). Errors and convergence order at final time t = 2 on nonuniform meshes.

We now take the step function

$$u(x,0) = \begin{cases} a, & x < 0.5, \\ b, & x > 0.5, \end{cases}$$
 (32)

as initial condition. The exact solution is

$$u(x,t) = a + \frac{b-a}{1+h(y,t)\exp\left(\frac{b-a}{2D}(y-ct)\right)}, \quad h(y,t) = \frac{1-\operatorname{erf}\left(\frac{y-at}{\sqrt{4Dt}}\right)}{1-\operatorname{erf}\left(-\frac{y-bt}{\sqrt{4Dt}}\right)}. \quad (33)$$

where y = x - 1/2 and c = (a + b)/2. We show the results in Fig. 3 with a = 1, b = 0.1, and D = 0.01. The iWENO3 scheme approximates the steep front very well.

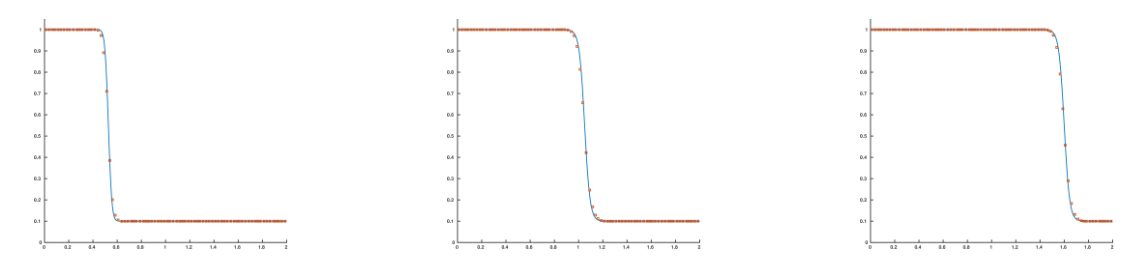


Fig. 3: Burgers' equation with initial condition (32). The blue solid line is the exact solution. The red open squares are our iWENO3 scheme with  $\Delta t = 4h$  on a nonuniform grid using m = 80 grid elements.

### **Example 3: Rigid Body Rotation.**

We consider rotation of a square patch on the unit square  $[0, 1]^2$ . The equation is

$$u_t - ((y - 1/2)u)_x + ((x - 1/2)u)_y = 0.$$
 (34)

We show the results in Fig. 4 after a rotation by angle  $\pi/4$  and  $\pi/2$  using  $\Delta t = 4\pi h$ . The scheme appears to give good results on an unstructured mesh, which is generated from an  $160 \times 160$  uniform rectangular mesh with edge length h by randomly perturbing the interior points within  $\pm 25\%$  of h, except the outer layer. The outer layer of elements is not perturbed, so as to facilitate the WENO reconstructions, which require a layer of ghost elements.

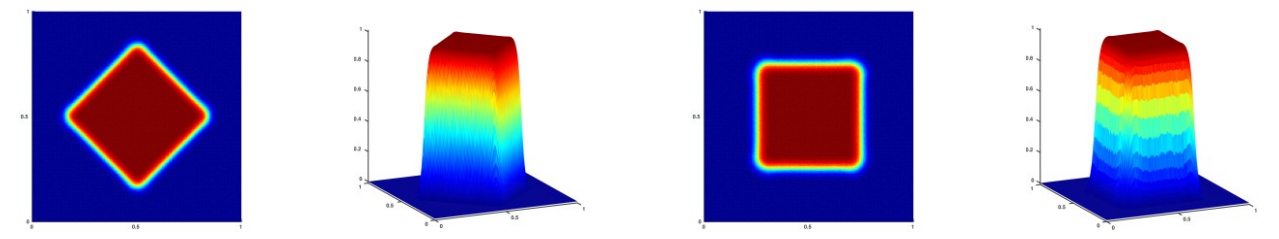


Fig. 4: Rigid body rotation using  $\Delta t = 4\pi h$  at  $t = \pi/4$  (left two figures) and  $\pi/2$  (right two figures).

### **Numerical Results for Two-Phase Flow**

In this section, we give results for our iWENO3 scheme applied to two-phase flow in a porous medium. We use the deal.ii package (Bangerth et al. 2015) to solve the mixed finite element method (5)-(6) for the pressure equation (using AC spaces). We use deal.ii's sparse direct solvers to solve the saturation equation (16)-(17), implementing no flow boundary conditions by reflection into boundary ghost cells.

We take  $\mathbf{g} = (0, 9.8 \text{m/s}^2)$ ,  $\phi = 0.3$ ,  $\rho_w = 1 \text{g/cm}^3$ ,  $\rho_n = 0.7 \text{g/cm}^3$ ,  $\mu_w = 0.5 \text{cp}$ , and  $\mu_n = 2.5 \text{cp}$  on  $m \times m$  unstructured meshes of quadrilaterals on the unit square reservoir domain 0 < x < 320 m and 0 < y < 320 m oriented vertically (i.e., y = z). We test using m = 16 and 50 grid elements in each direction, with the initial condition  $S_w = 0$ . The absolute permeabilities average about 66 mD and 40 mD, respectively, and they are shown in log scale in Fig. 5.

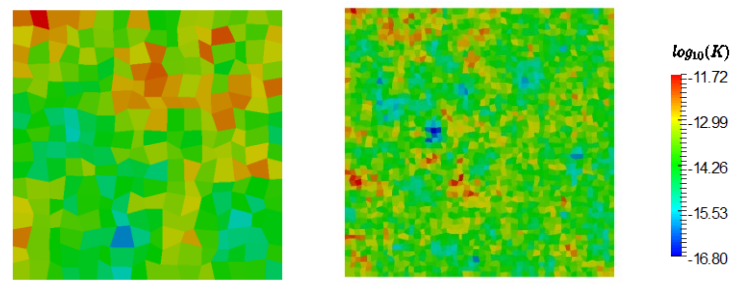


Fig. 5: Log<sub>10</sub> of absolute permeability ( $m^2$ ) for m = 16 (left) and m = 50 (right).

The Brooks and Corey model (Brooks & Corey 1964) gives the capillary pressure

$$p_c(S_w) = p_e S_w^{-1/\lambda}, \qquad (35)$$

where  $p_e$  is the entry pressure. The relative permeabilities are

$$k_{rw}(S_w) = S_w^{(2+3\lambda)/\lambda}, \quad k_{rn}(S_w) = (1 - S_w)^2 \left(1 - S_w^{(2+\lambda)/\lambda}\right). \quad \dots$$
 (36)

We take  $p_e = 3$ psi and  $\lambda = 2$ .

The wells are modeled by the well terms  $q_w(S_w)$  and  $q_n(S_w)$ . An injection well injects no nonwetting fluid, so  $q_n = 0$ , and wetting fluid at a rate of  $q_w = 1/\text{day}$  over the grid block for which it is active, so it injects a volume of about  $(320/m)^2/\phi$  m<sup>2</sup>/day (the grid blocks are not square, so this is only approximate). Production wells produce total fluid at the same total rate q = -1/day, and set  $q_w(S_w) = (\lambda_w(S_w) / \lambda(S_w))q$ .

All test examples run until the final time t = 600 days with an increasing  $\Delta t$ , starting with  $\Delta t = 0.5$  days until t = 10 days, then  $\Delta t = 1$  day until t = 50 days,  $\Delta t = 2$  days until t = 150 days,  $\Delta t = 5$  days until t = 200 days, and  $\Delta t = 10$  days until t = 600 days.

Our results at different times are shown in Figs. 6-10. We show in Fig. 6 the case with m = 16 and an injector in the top left and producer in the bottom right. We see a clean saturation profile. The top set of results use  $AC_0$  mixed spaces for the pressure equation, which give only first order accurate velocities. The bottom row shows results using  $AC_1$  mixed spaces, which are second order accurate. Some differences can be detected between the two tests, suggesting that it is important to compute the velocity to higher than first order.

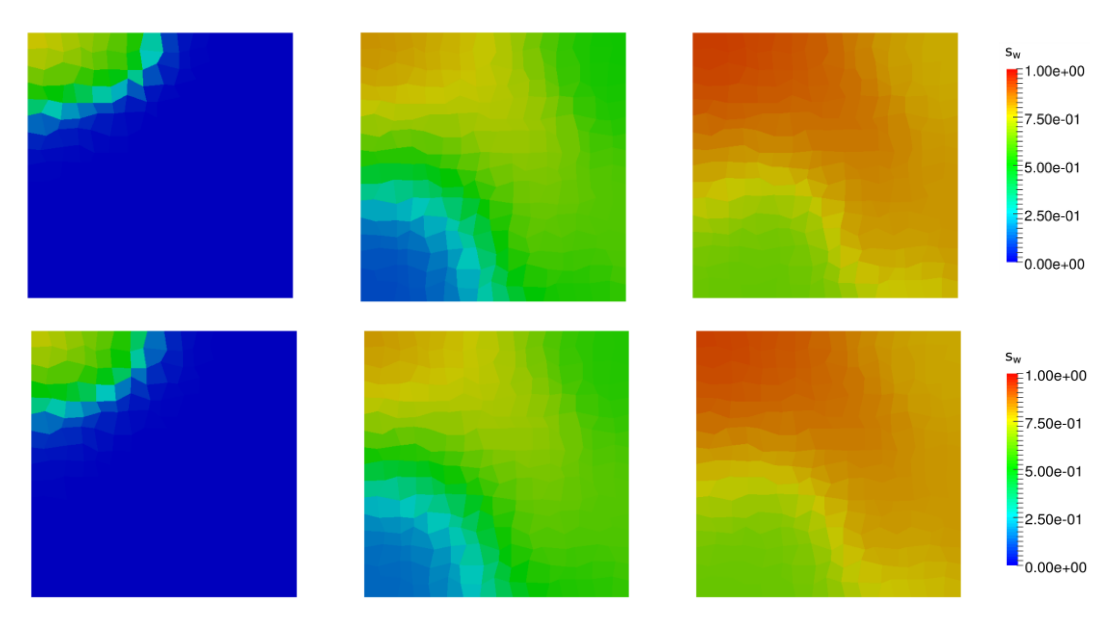


Fig.6: Saturation for m = 16 at t = 5, 50, 450 days.  $AC_0$  (top),  $AC_1$  (bottom).

In Fig. 7, we show that the scheme undershoots (black elements) a little at early time. In fact, a small wave is created near the steep front that propagates toward the production well. The minimal saturation is only about -3.1E-4 on the  $16\times16$  mesh, so the scheme is essentially nonoscillatory. This level of undershooting was about the same for our other tests. We did not detect saturation overshooting the value one in any of these tests. The selection of the parameter  $\epsilon$  in (19), which we took as 1E-6, is critical to these results, because  $\epsilon$  controls the identification of small oscillations that need to be damped.

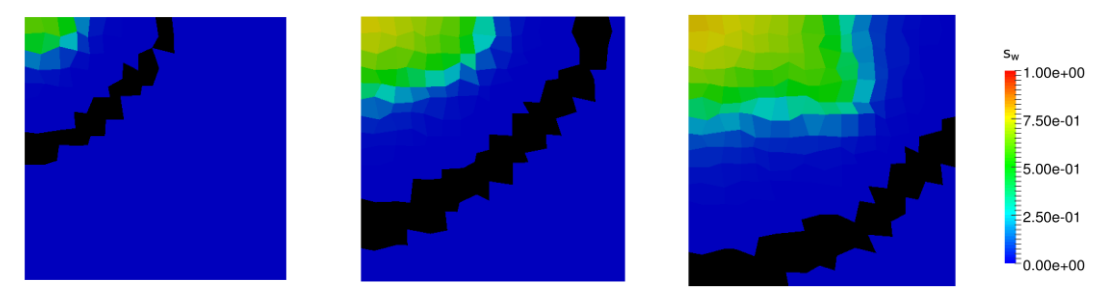


Fig.7: Saturation for m = 16 at t = 1, 10, 15 days. Black shows negative values.

We see similar results for the bigger example using m = 50 in Fig. 8. Again, some differences can be detected between using AC<sub>0</sub> and AC<sub>1</sub>, and overall a clean saturation profile is observed.

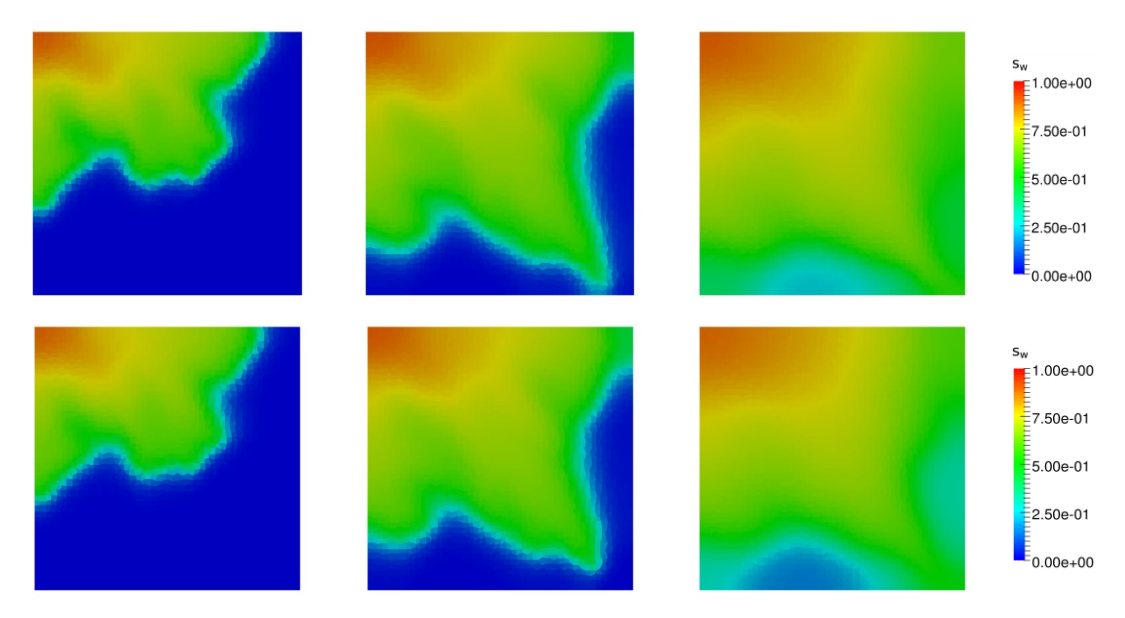


Fig. 8: Saturation for m = 50 at t = 200, 350, 600 days.  $AC_0$  (top),  $AC_1$  (bottom).

For Figs. 9 and 10, there are injection wells at the four corners cells, and four producer wells at each of the four center cells, mimicking a five-spot pattern (even though the reservoir is vertical). For these tests, we use AC<sub>1</sub> spaces for the pressure equation. Very clean results are obtained.

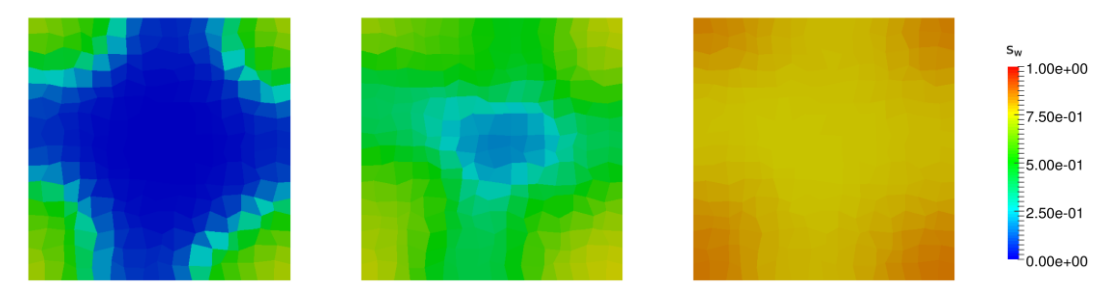


Fig. 9: Saturation for m = 16 at t = 4, 10, 90 days using AC<sub>1</sub>.

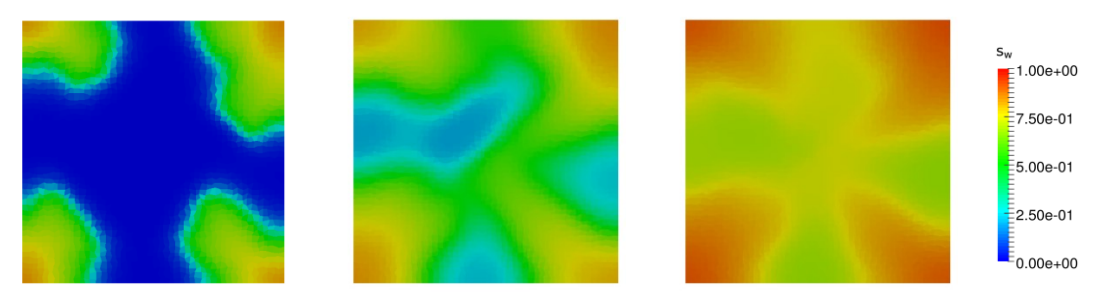


Fig.10: Saturation for m = 50 at t = 50, 110, 600 days using AC<sub>1</sub>.

## **Conclusions and Future Research**

The iWENO methodology provides a generalization of standard low-order finite volume schemes. Schemes can be defined to any order of accuracy on unstructured meshes in two or three space dimensions, with only a few unknowns per grid block per variable. An L-stable time integrator, such as Radau-IIA, is needed to make sure that iWENO is unconditionally stable when applied to the linear problem having a smooth solution. Advection, (capillary) diffusion, and wells can be approximated accurately by the scheme.

New AC mixed finite element spaces provide accurate velocities on quadrilateral meshes. It may be important to use more than first order accurate  $AC_0$  for high order approximation of the saturation.

WENO-AO reconstruction is highly advantageous over standard WENO reconstruction, since it gives a reconstruction that can be evaluated at any point and uses arbitrary positive weights. The WENO-AO reconstructions based on tensor product polynomials simplify the construction of the stencil polynomials and smoothness indicators, which can be defined in terms of base polynomials.

Future research directions include using the WENO framework to solve the pressure equation and systems of three phases such as compositional and black oil systems. More research is needed to extend the schemes to treat complex wells and multiple rock types, and to improve the satisfaction of the maximum principle.

### **Nomenclature**

 $D,\widehat{D}$  = diffusive flux and its Lax-Friedrichs flux,  $D = -K p_c' \lambda_w \lambda_n / \lambda$ 

ds = differential of length

E = computational mesh grid element (or cell, or block)

 $F,\hat{F}$  = hyperbolic flux and the Lax-Friedrichs flux for  $F \cdot v$ ,  $F = f_w u - \gamma g$ 

 $f_w =$  fractional flow of wetting fluid,  $f_w = \lambda_w / \lambda$ 

g = gravity vector

h = mesh spacing (maximal element diameter)

K = absolute rock permeability

L = number of facets of the boundary of E (here taken as 4)

P = polynomial approximation used in the WENO reconstructions

p =global pressure

 $p_c$  = capillary pressure

 $p_e, \lambda = \text{Brooks-Corey parameters}$ 

 $p_n,p_w$  = phase pressures

 $q_n, q_w = \text{wells}$ 

R = WENO reconstruction

 $S^{-}$ ,  $S^{+}$  = WENO reconstructed saturation values, defined from within and outside the mesh element

 $S_w$  = wetting fluid saturation

 $\bar{S}_E$  = average wetting fluid saturation over mesh element E

```
u = total velocity
```

 $\alpha, \tilde{\alpha}$  = linear and nonlinear WENO weights

 $\gamma = \text{gravity term}, \ \gamma = K (\rho_n - \rho_w) \lambda_w \lambda_n / \lambda \delta$ 

 $\Delta t = \text{time step duration}$ 

 $\delta$  = parameter in Lax-Friedrichs flux

 $\partial E_l = l$ -th facet of the boundary of element E

 $\varepsilon$  = small parameter in nonlinear WENO weighting

 $\lambda = \text{total mobility}, \lambda = \lambda_n + \lambda_w$ 

 $\lambda_n$ ,  $\lambda_w$  = phase mobilities (relative permeability divided by viscosity)

 $\mu_n, \mu_w = \text{phase viscosities}$ 

 $\nu$  = outer unit normal vector

 $\rho$  = density term,  $\rho = (\lambda_w \rho_w + \lambda_n \rho_n) / \lambda$ 

 $\rho_n, \rho_w =$  phase densities

 $\sigma$ = smoothness indicator

 $\omega$  = quadrature weight

# **Acknowledgments**

The work of the first author was supported in part by the U.S. National Science Foundation grant DMS-1720349. The work of the second author was supported in part by the Taiwan Ministry of Science and Technology grant MOST 107-2115-M-110-004-MY2, National Center for Theoretical Sciences, Taiwan, and the Multidisciplinary and Data Science Research Center of the National Sun Yat-sen University. The work of the third author was supported in part by the U.S. National Science Foundation grant DMS-1418752.

### References

Alpak, F.O. (2007, January 1). A Mimetic Finite Volume Discretization Operator for Reservoir Simulation. Society of Petroleum Engineers. doi:10.2118/106445-MS

Alpak, F.O. (2010, June 1). A Mimetic Finite Volume Discretization Method for Reservoir Simulation. Society of Petroleum Engineers. doi:10.2118/106445-PA

Aràndiga, F., Baeza, A., Belda, A.M. & Mulet, P. (2011). Analysis of WENO schemes for full and global accuracy, SIAM J. Numer. Anal. 49 (2):893-915.

Arbogast, T. (1992). The existence of weak solutions to single-porosity and simple dual-porosity models of two-phase incompressible flow, *J. Nonlinear Analysis: Theory, Methods, and Applications*, **19**:1009-1031.

Arbogast, T. & Correa, M.R. (2016). Two families of H(div) mixed finite elements on quadrilaterals of minimal dimension, SIAM J. Numer. Anal. 54(6):3332-3356, DOI 10.1137/15M1013705.

Arbogast T., Huang, Ch.-S. & Zhao, X. (2018). Accuracy of WENO and Adaptive Order WENO Reconstructions for Solving Conservation Laws, SIAM J. Numer. Anal. 56 (3):1818-1847.

Arbogast T., Huang, Ch.-S. & Zhao, X. (2018, March 30). Von Neumann Stable, Implicit Finite Volume WENO Schemes for Hyperbolic Conservation Laws, Technical Report18-04, Institute for Computational Engineering and Sciences, Univ. of Texas at Austin.

Arbogast, T. & Tao, Z. (2019). Direct serendipity and mixed finite elements on convex quadrilaterals. Submitted, preprint arXiv:1809.02192.

Arbogast, T. & Tao, Z. (2018, to appear). Construction of H(div)-conforming mixed finite elements on cuboidal hexahedra, *Numer. Math.* DOI 10.1007/s00211-018-0998-7.

Bangerth, W., Heister, T., Heltai, L., Kanschat, G., Kronbichler, M., Maier, M., Turcksin, B., & Young, T.D. (2015). The deal.II Library, Version 8.2, *Archive of Numerical Software* 3:1-8.

Brooks, R.H. & Corey, A.T. (1964). Hydraulic Properties of Porous Media. Hydrology Papers 3, Colorado State Univ., Fort Collins, p. 27. Chavent, G. & Jaffré, J. (1986). Mathematical models and finite elements for reservoir simulation, New York: Elsevier Science Publishers.

Chen, Q.-Y., Mifflin, R. T., Wan, J., & Yang, Y. (2007, January 1). A New Multipoint Flux Approximation for Reservoir Simulation. Society of Petroleum Engineers. doi:10.2118/106464-MS

Chen, Z., Huan, G., & Ma, Y. (2006). Computational Methods for Multiphase Flows in Porous Media, Philadelphia: SIAM.

Durlofsky, L.J., & Chien, M.C.H. (1993, January 1). Development of a Mixed Finite-Element-Based Compositional Reservoir Simulator. Society of Petroleum Engineers. doi:10.2118/25253-MS

Gaël, G., Benoît J., et al. (2010). Eigen v3. http://eigen.tuxfamily.org.

Gottlieb, S. (2005). On High Order Strong Stability Preserving Runge-Kutta and Multi Step Time Discretizations, *J. Sci. Comput.* **25** (1-2): 105-128, DOI: 10.1007/s10915-004-4635-5.

Gottlieb S., Shu, C.-W. & Tadmor, E. (2001). Strong stability preserving high-order time discretization methods, SIAM Review 43:73-85.

- Guevara-Jordan, J. M., & Jhonnanthan, A.-A. (2007, January 1). A Second-Order Mimetic Approach for Tracer Flow in Oil Reservoirs. Society of Petroleum Engineers. doi:10.2118/107366-MS
- Hairer, E., Lubich, C. & Wanner G. (2006). Geometric Numerical Integration: Structure-Preserving Algorithms for Ordinary Differential Equations, 2<sup>nd</sup> ed. Berlin, New York: Springer-Verlag. ISBN 978-3-540-30663-4.
- Hairer, E. & Wanner G. (1996). Solving Ordinary Differential Equations II: Stiff and Differential-Algebraic Problems, 2<sup>nd</sup> ed. Berlin, New York:Springer-Verlag. ISBN 978-3-540-60452-5.
- Harten, A., Engquist, B., Osher, S. & Chakravarthy S. R. (1987). Uniformly high-order accurate essentially nonoscillatory schemes III, *J. Comput. Phys.* **71** (2):231-303
- Hoteit, H. & Firoozabadi, A. (2008). An efficient numerical model for incompressible two-phase flow in fractured media, *Advances in Water Resources* **31** (6):891-905.
- Hu, C. & Shu, C.-W. (1999). Weighted essentially non-oscillatory schemes on triangular meshes, J. Comput. Phys., 150:97-127.
- Jiang G.-S. & Shu, C.-W. (1996). Efficient implementation of weighted ENO schemes, J. Comput. Phys 126: 202-228.
- Ketcheson, D. I., Macdonald, C. B. & Gottlieb S. (2009). Optimal implicit strong stability preserving Runge-Kutta methods, *Applied Numerical Mathematics* **59**:373-392.
- Lake, L.W. (1989). Enhanced Oil Recovery, Englewood Cliffs, New Jersey: Prentice Hall.
- Lee, S. & Wheeler, M. F. (2017). Adaptive enriched Galerkin methods for miscible displacement problems with entropy residual stabilization, *J. Comput. Phys.* **331**:19-37.
- Levy D., Puppo G. & Russo G., Central WENO schemes for hyperbolic systems of conservation laws, *Math. Model. Numer. Anal.* 33:547-571.
- Liu, X. D., Osher S. & Chan T. (1994). Weighted essentially non-oscillatory schemes, J. Comput. Phys. 115:200-212.
- Mallison, B., Gerritsen, M., Jessen, K., & Orr, F. M. (2003, January 1). High Order Upwind Schemes for Two-Phase, Multicomponent Flow. Society of Petroleum Engineers. doi:10.2118/79691-MS
- Nilsen, H.M., Natvig, J.R., & Lie, K.-A. (2012, June 1). Accurate Modeling of Faults by Multipoint, Mimetic, and Mixed Methods. Society of Petroleum Engineers. doi:10.2118/149690-PA
- Parramore, E., Edwards, M. G., Lamine, S., & Pal, M. (2013, February 18). Multiscale Formulations with CVD-MPFA Schemes on Structured and Unstructured Grids. Society of Petroleum Engineers. doi:10.2118/163626-MS
- Peaceman, D. W. (1977). Fundamentals of Numerical Reservoir Simulation. Amsterdam: Elsevier.
- Riviere, B., Chidyagwai, P., & Mishev, I. D. (2011, January 1). On the Coupling of Finite Volume and Discontinuous Galerkin for Reservoir Simulation Problems. Society of Petroleum Engineers. doi:10.2118/141971-MS
- Russell, T. F. & Wheeler, M. F. (1983). Finite element and finite difference methods for continuous flows in porous media, Chapter II in The Mathematics of Reservoir Simulation, R. E. Ewing (ed.), Philadelphia: Society for Industrial & Applied Mathematics.
- Souza, M.R.A., Contreras, F.R.L., Lyra, P.R.M., & Carvalho, D.K.E. (2018, Dec. 1). A Higher-Resolution Flow-Oriented Scheme With an Adaptive Correction Strategy for Distorted Meshes Coupled With a Robust MPFA-D Method for the Numerical Simulation of Two-Phase Flow in Heterogeneous and Anisotropic Petroleum Reservoirs. Society of Petroleum Engineers. doi:10.2118/182677-PA
- Titarev, V.A., Tsoutsanis, P. & Drikakis, D. (2010). WENO schemes for mixed-element unstructured meshes, *Commun. Comput. Phys.* 8: 585-609.
- Wang, K., Zhang, L., & Chen, Z. (2015, October 20). Development of Discontinuous Galerkin Methods and a Parallel Simulator for Reservoir Simulation. Society of Petroleum Engineers. doi:10.2118/176168-MS
- Wheeler, M.F., Xue, G., & Yotov, I. (2012, September 1). Accurate Cell-Centered Discretizations for Modeling Multiphase Flow in Porous Media on General Hexahedral and Simplicial Grids. Society of Petroleum Engineers. doi:10.2118/141534-PA
- Zidane, A., & Firoozabadi, A. (2018, September 24). Efficient Simulation of Two-Phase Compositional Flow in Fractured Reservoirs Using 3D Unstructured Gridding in Complex Geometries. Society of Petroleum Engineers. doi:10.2118/191405-MS